NASA

Technical Memorandum 85055

Currents in Saturn's Magnetosphere

J. E. P. Connerney, M. H. Acuna,
and N. F. Ness

JUNE 1983

National Aeronautics and
Space Administration

Goddard Space Flight Center
Greenbelt, Maryland 20771

CURRENTS IN SATURN'S MAGNETOSPHERE

J. E. P. Connerney, M. H. Acuna, N. F. Ness
NASA/Goddard Space Flight Center
Laboratory for Extraterrestrial Physics
Greenbelt, Maryland 20771

Abstract

A model of Saturn's magnetospheric magnetic field is obtained from the Voyager 1 and 2 observations. A representation consisting of the Z_3 zonal harmonic model of Saturn's planetary magnetic field together with an explicit model of the equatorial ring current fits the observations well within $r < 20$ R_s, with the exception of data obtained during the Voyager 2 inbound pass. The exception is attributed to a time variation of Saturn's magnetosphere driven by a drop in solar wind ram pressure. The magnetohydrodynamic momentum equation is used to obtain, from the magnetic field model, estimates of the plasma pressure and mass density at radial distances of $8 < r < 16$ R_s. These estimates are generally consistent with those obtained by the Pioneer 11 and Voyager plasma investigations. The Voyager 1 observations suggest the presence of a global field aligned current of $\sim 10^7$ A flowing into the (southern) auroral zone in the evening sector. No evidence of such a field aligned current system is found in the Voyager 2 observations obtained a year later.

The Pioneer 11 magnetic field investigations revealed a dipolar planetary magnetic field of moment ~ 0.20 G - R_S^3, aligned to within $\sim 1°$ of Saturn's rotation axis and apparently offset along the axis to the north by .04 [Acuña et al., 1980] or .05 R_S [Smith et al., 1980]. However, the pre-encounter discovery by the Voyager Planetary Radio Astronomy team [Kaiser et al., 1980] of a modulation of Saturn's radio emissions suggested an anomaly in or a tilt of Saturn's magnetic field with respect to the rotation axis. The Voyager 1 observations confirmed the Pioneer 11 estimate of the magnetic moment ($\sim .21$ G-R_S^3) and the small tilt ($< 1°$) of Saturn's dipole but were not consistent with the offset dipole model [Ness et al., 1981; Acuña et al., 1981]. The Voyager 1 observations did reveal the presence of a large-scale azimuthal equatorial ring current system [Ness et al., 1981; Connerney et al., 1981] and associated centrifugal plasma loading of Saturn's magnetosphere. The distortion of Saturn's magnetosphere was also inferred from a satellite absorption feature observed near the orbital position of Rhea (8.78 R_S) by the cosmic ray experiment [Vogt et al., 1981]. This signature was subsequently shown to be quantitatively consistent with the ring current model magnetosphere derived from the Voyager 1 magnetic field observations [Connerney et

al., 1981b]. In terms of geometry, Saturn's magnetosphere appeared intermediate to those of Earth and Jupiter; a magnetosphere that perhaps lacked the size and plasma pre-requisite to the formation of a Jovian-like magnetodisc.

The Voyager 2 observations of Saturn's magnetosphere [Ness et al., 1982], in conjunction with the complementary observations obtained by Voyager 1, led to a resolution of the seemingly disparate views of the planetary magnetic field with the introduction of the Z_3 zonal harmonic model [Connerney et al., 1982]. The continued presence of Saturn's ring current was noted [Ness et al., 1982] and suggested a relatively stable magnetospheric geometry against which the more time variable aspects of Saturn's magnetosphere [Ness et al., 1982 Bridge et al., 1982; Krimigis et al., 1982] could be viewed. There was no evidence in the Voyager magnetic field observations of the quasi-periodic outflow of plasma and consequent magnetospheric reconfiguration anticipated [Frank et al., 1980] from Pioneer 11 observations of a high β plasma near 6.5 R_S.

Using the Z_3 description of Saturn's planetary magnetic field, we re-examine the V1 and V2 observations to obtain an improved model ring current and magnetosphere. Inferences regarding the gross properties of the plasma entrapped in the magnetosphere are drawn from the model magnetosphere using magnetohydrodynamic stress balance for a centrifugally distorted magnetosphere. Evidence is found in the Voyager 1 observations suggesting a high (southern) latitude current system active during the Voyager 1 encounter but dormant during the Voyager 2 encounter a year later.

The axisymmetry of Saturn's planetary magnetic field, evident in the magnetic field data and the charged particle absorption signatures created by the satellites and rings [Simpson et al., 1980; McDonald et al., 1980; Vogt et al., 1982], presents an observational limitation to in situ magnetospheric investigations conducted by flyby spacecraft. The encounter trajectories of Pioneer 11, Voyager 1 and Voyager 2 are illustrated in Figure 1 in a planet centered cylindrical coordinate system. As the rotational and magnetic axes are identical, the Voyagers sampled but two magnetic latitudes at each radius, one inbound and one outbound from periapsis. Pioneer 11 sampled along

a nearly identical near-equatorial swath both inbound and outbound. Both Pioneer 11 and Voyager 2 spent much of the encounter at constant magnetic latitudes. As a result of the axisymmetry of the magnetic field and the flyby encounters, inferences about the distribution of currents and charged particles throughout the magnetosphere rely heavily on the differences observed between the inbound and outbound portions of the trajectories. It is particularly difficult to distinguish spatial variations from temporal variations occurring during the encounter; intercomparison between the encounters is likewise complicated by probable time variations linked to changes in the solar wind properties.

Ring Current Model

A useful and revealing presentation of the magnetic field data for studies of magnetic fields of external origin is that of a perturbation magnetic field plot. The perturbation field $\Delta\bar{B}$ is the difference between the observed magnetic field at any position and the predicted magnetic field of internal origin, obtained by subtracting from the observations a model internal field. The model adopted herein is the Z_3 zonal harmonic model of Saturn's planetary magnetic field deduced from Voyager 1 and 2 observations [Connerney et al., 1982]. The axisymmetric, octupole Z_3 model is characterized by the three Schmidt-normalized spherical harmonic coefficients g_1^0 = 21,535 nT, g_2^0 = 1642 nT and g_3^0 = 2743 nT. The internal field is thus confined to meridional planes and any observed azimuthal magnetic field component is of external origin.

The perturbation field plot of the Voyager 2 magnetic field observations shown in Figure 2 illustrates well the basic features of the external field. Each perturbation field component is shown on a common scale of ± 20 nT for a two day period centered about the V2 closest approach (CA) at 2.69 R_s which occurred at 0324, day 238. The last (inbound) observed bow shock (BS) at 0026, day 237 and only (inbound) observed magnetopause (MP) at 0700 day 237 [Ness et al., 1982] are indicated in addition to three relatively brief spacecraft roll maneuvers (stippled). Data obtained during the roll maneuvers has been deleted because the reconstruction of the spacecraft attitude, during the rolls, has an angular accuracy of ~ 2° as compared with ~ 0.2° achieved

otherwise. The maximum field magnitude of 1187 nT was observed at 0304 day 238, just prior to closest approach. The external field at this time is ~ 1% of the total observed magnetic field. Thus even small inaccuracies in either the internal magnetic field (removed from the observations) or the spacecraft orientation (e.g., during a spacecraft roll) would result in a large and localized departure of the perturbation field curve from that shown.

A most remarkable feature of the V2 observations is the lack of an appreciable azimuthal magnetic field component. The ΔB_ϕ illustrated in Figure 2 is the entire observed azimuthal field, since the Z_3 internal field does not have an azimuthal component. It is everywhere small (< 5 nT) and not simply related to the spacecraft radial range. In the θ and r components of the perturbation field plot the characteristic features of a ring current are evident. Along the V2 trajectory (Figure 1) the θ component of the external field increases slowly with decreasing spacecraft radial range, oppositely directed to the equatorial planetary field. The radial field component of the external field, also slowly varying, reaches a maximum at $5 < r < 10\ R_S$ and reverses sign as V2 crosses the equator at 0418, day 238.

Also shown in Figure 2 is the computed external magnetic field of the model ring current fitted to both V1 and V2 observations. In this model, large-scale azimuthal currents flow eastward in an annular disk extending from 8 R_S to 15.5 R_S in Saturn's equatorial plane. The current is assumed to be distributed uniformly in $\hat{z}$ throughout the total disk thickness of 6 R_S and decreases with radial distance from Saturn, i.e.,

$$J_\phi = I_o/\rho \qquad 8\ R_S < \rho < 15.5\ R_S \qquad |z| < 3$$

$$J_\phi = 0 \qquad \text{elsewhere}$$

where $I_o = 2.9 \times 10^6$ A/R_S; 1 R_S = 60,330 km. The current density decreases from 0.36×10^6 A/R_S^2 (0.10 mA/km^2) at 8 R_S to 0.19×10^6 A/R_S^2 (0.05 mA/km^2) at 15.5 R_S. These model parameters, selected to best fit the combined Voyager 1 and Voyager 2 data sets, are very similar to those obtained from the V1 observations alone [Connerney et al., 1981] prior to the V2 encounter. In

order to better fit the V2 observations, the inner edge of the ring current has been decreased by 0.5 R_S to 8.0 R_S and the half thickness increased by 0.5 R_S to 3.0 R_S. The current density is unchanged but the total integrated ring current increases (by $\sim$ 1/3) to 11.5 x 10^6 A.

Implicit in the above is the assumption that differences in the V1 and V2 observations reflect spatial and not temporal variations. Within the context of the present model, the V1 and V2 observations are represented to an equal approximation by the same ring current, i.e., no significant improvement in the model fits can be obtained by introducing different ring currents for the two encounters. However, the observations are not inconsistent with relatively small differences in ring current geometry and intensity between the two encounters. This possibility was examined by fitting the combined Voyager 1 and 2 data sets to a model consisting of a planetary field and a time-variable external field. The planetary field was represented by a zonal harmonic expansion, characterized by the Schmidt coefficients g_1^0, g_2^0, and g_3^0. The external field, attributed primarily to the ring current, was approximated by an external spherical harmonic expansion of order 1 (G_1^0, G_1^1, H_1^1), equivalent to a (spatially) uniform external field. The external field was allowed to assume different values for each of the two encounters. The results are summarized in Table 1 and compared with the Z_3 model field. The difference in the axially symmetric part of the external field (G_1^0) for the two encounters is small. This difference may be due to the use of a uniform external field approximation and the different trajectories of Voyager 1 and 2. Voyager 1 remained closer to the equator than did Voyager 2 (Figure 1). At higher latitudes, less of the ring current perturbation field appears in the θ component. This may be sufficient to account for the lesser G_1^0 obtained for the Voyager 2 flyby (-9 nT) compared to Voyager 1 (-11 nT).

This ring current model is a suitably scaled replica of that used to model the Jovian magnetodisc [Connerney et al., 1981]. In contrast to the sheet-like geometry of Jupiter's magnetodisc currents, the principal current-carrying region of Saturn's magnetosphere is thicker, relative to its radial extent. Actual current densities in Saturn's magnetosphere are an order of magnitude less than those in the Jovian magnetosphere at comparable radial distances.

Presented in Figure 3 in the same perturbation field format described earlier are the Voyager 1 magnetic field observations at Saturn. All five observed (inbound) magnetopause (MP) boundaries, occurring between 0154 and 0247, day 317 [Ness et al., 1981] are indicated along with two spacecraft roll maneuvers (stippled) executed following closest approach (C.A.). The maximum field magnitude of 1093 nT, measured just before closest approach, is comparable to that measured by V2 during its encounter. The relative magnitude of the internal and external field is thus similar for the two encounters. While the inferred V1 external field is generally similar to that of V2, a comparison of the V1 (Figure 3) and V2 (Figure 2) perturbation fields, with reference to Figure 1 for trajectory information, reveals interesting differences related to the different Voyager trajectories. Most evident in the Voyager 1 data is the relatively large azimuthal field component, increasing with decreasing radial range of the spacecraft, and the coincident bipolar features occurring in the θ and r components. A discussion of this interesting feature is deferred to the next section.

Voyager 1's more nearly equatorial passage inbound towards periapsis on day 317 reveals a localized field enhancement at a radial distance of $\sim$ 15 R_S, as Voyager 1 passed over the outer edge of the ring current. The lack of an observable edge effect in the outbound Voyager 1 ΔB_θ is a simple consequence of V1's greater latitude outbound. Voyager 2 was even more distant from the equatorial plane during passage through the middle and outer magnetosphere and as such recorded only the smooth variation of the external field due to distant currents. In the Voyager 1 outbound data, the maximum external field of $\sim$ 12.5 nT is observed as Voyager traverses the inner edge of the ring current at $\sim$ 8 R_S, again at relatively low latitude. As Voyager 1 progresses further outbound, a maximum in the radial field component marks approximately the spacecraft emergence from the current-carrying region.

The geometrical extent of the ring current deduced from the magnetometer observations roughly corresponds to the boundaries of the 'extended plasma sheet' described by Bridge et al. [1981; 1982]. Bridge et al. [1982] concluded that the extended plasma sheet observed by Voyager 2 was similar to that observed by Voyager 1 except that: 1) the inner edge of the sheet was

observed at L ~ 6 (V2) rather than L ~ 8 (V1); and 2) the sheet half-thickness during the V2 encounter (5 R_S) was considerably greater than that inferred from the Voyager 1 observations (~ 2 R_S). The Voyager 2 magnetic field observations, more distant from the equatorial plane, are relatively insensitive to the position of the inner edge of the ring current and therefore cannot be used to identify such a shift in the inner edge of the ring current. However, the magnetic field data are most consistent with the 6 R_S thickness and are not compatible with a uniform distribution of the ring current over a 10 r_S thick torus. Sittler et al. [1981] have noted that the inner edge of the ring current at 8 R_S coincides with the radial extent of the E-ring deduced from the extinction of suprathermal electrons and optical observations [Baum et al., 1981]. They suggest that the E ring neutral gas and dust is likewise responsible for the extinction of the prominent ring current carriers at the inner boundary of the ring current. The outer boundary at 15.5 R_S is also close to the outer extremity (17 R_S) of the region of stable trapping discussed by Krimigis et al. [1981].

The only significant disagreement between the Voyager 2 perturbation field and the ring current model magnetic field occurs during the inbound pass, concomitant with highly variable plasma electron densities [Bridge et al., 1982] and disturbed electron and ion anisotropies [Krimigis et al., 1982]. Ness et al. [1982] argued that the major expansion of Saturn's magnetosphere, necessary to reconcile the magnetopause boundaries observed inbound with those observed outbound, occurred during hours 1000 to 1600, day 237. The discrepancy between the modeled external field and that observed during this period and shortly thereafter is regarded as a result of the magnetospheric expansion and consequent temporary disruption of the ring current.

An Auroral field Aligned Current?

The remaining feature evident in the V1 perturbation field plot (Figure 3) is the comparatively large azimuthal field component (which reaches a maximum near closest approach) and the coincident bipolar disturbance appearing in the theta and radial components. We argue that this feature, manifested in all three components of the Voyager 1 magnetic field data, is

not directly related to either the planetary field or the ring current. A plausible explanation is offered in terms of a field aligned current system linking Saturn's southern auroral zone with the distant magnetosphere.

It is most convenient to examine the ΔB_ϕ component of the perturbation plot in detail since neither the model ring current nor planetary field contribute to the azimuthal field. The maximum azimuthal field is observed not at the minimum planetocentric radial distance but rather just before closest approach at the minimum axial distance ρ. In Figure 4 the observed azimuthal field is replotted as a function of axial distance ρ demonstrating not only the large scale length of the feature but a remarkable linear dependence on $1/\rho$ of the field amplitude over a radial range of $\sim$ 10 R_S. The dashed line in Figure 4 is computed using B_ϕ (nT) = [33.30/ρ] - 4.62, with ρ in units of planetary radius, obtained by least-squares fit of the azimuthal field within 10 R_S (excluding data obtained during the roll maneuver, indicated in Figure 4). In Figure 5 the Voyager 1 azimuthal field vectors are shown along the equatorial plane projection of the spacecraft trajectory in local time. The trajectory of Voyager 2 is indicated in Figure 5 as well but the azimuthal field vectors have been omitted for clarity. The azimuthal field observed by Voyager 2 was small throughout encounter and apparently unrelated to the spacecraft radial range (see Figure 2).

It is highly unlikely that the observed azimuthal field is generated by a system of currents internal to Saturn. Currents completely confined within some radius r^* smaller than the V1 close approach radial distance of 3.07 R_S would result in a magnetic field at $r > r^*$ expressible as a sum of terms with r^{-n} radial dependence where $n \geq 3$. A $1/\rho$ dependence of the azimuthal field amplitude over $\sim$ 10 R_S radial distance and $\sim$ 1.5 Saturn rotations cannot reasonably be constructed by a superposition of such terms. Nor is there any indication in the Voyager 2 observations obtained a year later (Figure 2) of a similar feature. We conclude that the V1 azimuthal field signature is generated by a large-scale magnetospheric current (system) active during the V1 encounter with Saturn in November 1980 and inactive during the V2 encounter in August 1981.

A simple conceptual model current system with the desired characteristics consists of a single infinite line current at the origin coaxial with Saturn's rotational and magnetic axes. From the coefficient 33.3 nT-R_S, $\sim 10^7$ A of current flowing south to north through Saturn's poles is required to obtain the part of the observed azimuthal field represented by the first term of the least squares fit. In this approximation, the second (constant) term of the least squares fit is attributed to distant magnetopause and/or magnetotail currents. A co-axial infinite line current contributes only to the azimuthal field component, however. Selecting instead a current path along a dipole field line it is possible to qualitatively match the scale length, relative amplitude, and polarity of the ΔB_θ and ΔB_r signatures as well if an auroral field line at $\sim$ 21.3 hrs local time is chosen.

The current system illustrated in Figure 6 incorporates the desired characteristics of the auroral current described above but is more realistic in providing continuity of current across the polar cap rather than through the planet. Figure 6 is a view of Saturn's south pole as it appeared to Voyager 1 at $\sim$ hour 2200 Day 317, schematically indicating the model field aligned current system. This model current system is confined to the southern hemisphere. A 9×10^6 A Birkeland current flows into the southern auroral zone at $\sim 80^\circ$ south latitude and 21.3 hours local time. The current closes along a highly conducting auroral path and exits in the early morning sector. Figure 7 illustrates the perturbation field observed by Voyager 1, and a model field consisting of the ring current field combined with that of the putative auroral field aligned current. The qualitative agreement between the computed and observed field is only suggestive of the field aligned current geometry of Figure 6. While the existence of a current system carrying $\sim 10^7$ A (net) at high latitudes into Saturn's south pole is relatively well established, the detailed geometry and location of that system is not well determined. For example, by distribution of the current over a range of local times in the early evening sector (centered about 21.3 hrs local time) the same scale length and amplitude observed in ΔB_r and ΔB_θ can be obtained with a less intense current system at sub-auroral latitudes. The early morning return path in particular is included in the model to satisfy a requirement for current continuity only, as the magnetic field observations are relatively insensitive to the path of this return current. The observations are likewise

insensitive to the auroral path, allowing an eastward or westward auroral electrojet or closure directly across the polar cap.

We have chosen the model illustrated in Figure 6 as the simplest single line current model consistent with the observations and the concept of field-aligned current flow (and enhanced polar conductivity). Since it is impossible to uniquely determine the distribution of current from magnetic field observations obtained outside the region of current flow, the proposed model is but one of many possibilities. In particular, the close-in Voyager 1 observations were obtained at southern latitudes and are therefore more sensitive to Birkeland currents located in the southern hemisphere. We do not speculate on the existence of a similar current system in the northern hemisphere.

The proposed current system may only represent a net imbalance between inflowing and outflowing auroral currents as suggested for the earth's auroral current systems (e.g., Heelis [1982]). Several $x10^6$ A of current flowing into and out of the earth's polar auroral zone have been identified by analysis of ground based and satellite observations [Iijima and Potemra, 1976]. The distribution and magnitude of the earth's auroral currents depend on the season as well as the interplanetary magnetic field direction and solar wind conditions [Heelis, 1982]. Many of the salient features of the earth's auroral current system can be understood on the basis of the 'open' magnetosphere model introduced by Dungey [1961]. In this model, the electric field across the earth's polar cap (20 $\sim$ 100 kv) is generated by the motion of the solar wind ($\sim$300 km/sec) past magnetic field lines ($\sim$ 5 nT) anchored in the polar ionosphere (see, e.g., Stern [1977; 1982]). If a similar solar dynamo operates at Saturn, it could be expected to generate 100 $\sim$ 500 kv across Saturn's polar cap, taking into account a lesser field strength (1 nT) and the relative size of the magnetospheres (25). With this EMF, an auroral (Hall and/or Pedersen) conductivity Σ_{sa} of order 10 mhos would be sufficient to conduct the inferred $\sim$ 9 x 10^6 A across Saturn's polar cap. Atreya et al. [in press] estimate the height integrated Pedersen conductivity of Saturn's auroral ionosphere to be Σ_{sa} = 58 mhos comparable to the earth's auroral conductivity [Heelis, 1982], and and in excess of that required.

The direction of current flow is also consistent with that expected of a solar wind dynamo. The solar wind dynamo would impose a dusk to dawn electric field across Saturn's polar caps. With the magnetic field directed into the south polar cap, Hall currents in the direction of $\vec{B}\times\vec{E}$ flow from midnight to noon across the polar cap. Adding a Pedersen current in the direction of $\vec{E}$ results in a net current flow across the pole from the pre-midnight sector to the early morning sector. If such a current is sustained by field-aligned currents into the polar region in the evening sector and out of the polar region in the morning sector, the resulting current flow in the southern hemisphere is similar to that inferred from the Voyager 1 magnetic field observations (Figure 6).

The solar dynamo model is consistent with both the magnitude and direction of the inferred current flow. However, a simple solar dynamo would be expected to operate equally well in the northern hemisphere, neglecting hemispherical asymmetries. We find no evidence in the Voyager 1 observations for a similar Birkeland current system in the northern hemisphere. The lack of such evidence may reflect the sampling bias of the Voyager 1 trajectory, a time variation of the solar wind conditions during encounter, a real hemispherical asymmetry in the solar wind interaction with the magnetosphere, or a failure of the solar dynamo model in this application. With the data available it does not seem possible to distinguish among the alternatives.

Association of the inferred current system with a solar wind dynamo, or at least an energy source ultimately related to the solar wind interaction with Saturn's magnetosphere, suggests a plausible explanation for the lack of evidence for a similar current system in the Voyager 2 observations. During the Voyager 2 encounter with Saturn, the magnetosphere grew in size [Ness et al., 1982; Bridge et al., 1982] indicative of a precipitous drop in solar wind ram pressure. More importantly, Warwick et al. [1982] and Scarf et al. [1982] reported the disappearance of Saturn kilometric radiation (SKR) for a period of several days during the Voyager 2 encounter. They suggested that during this time, Saturn's magnetosphere might have been enveloped in Jupiter's magnetic tail (or a tail filament) and thus removed from the solar wind. Since SKR originates on auroral field lines (near noon or the dayside cusp in

the northern hemisphere; [Kaiser and Desch, 1982]) and is heavily influenced by the solar wind [Desch, 1982], the presence of SKR is rather directly indicative of polar access to a solar wind dynamo. Its absence during the Voyager 2 encounter suggests the removal of the solar wind dynamo and the associated Birkeland current system. The presence or absence of a similar current system operative during the Pioneer 11 encounter with Saturn cannot be determined from the fluxgate magnetometer observations [Acuña and Ness, 1979] owing to a relatively large digitization uncertainty nor from the published accounts of the vector helium magnetometer experiment [Smith et al., 1980].

Another current system capable of reproducing the azimuthal field radial dependence has received some consideration in the context of the Pioneer magnetic field observations at Jupiter [Parish et al., 1980; Connerney, 1981; Thomsen and Goertz, 1981] and the outward transport of angular momentum in the Jovian magnetosphere [Hill, 1979; 1980]. This system retains the field-aligned current flow into the polar region (at sub-auroral latitudes, however) but closes along field lines at lower latitudes equatorward at all longitudes and thereafter exits radially outward in the equatorial plane. Angular momentum is transferred to equatorial plasma by local $\vec{j}x\vec{B}$ forces at the expense of ionospheric angular momentum lost in a sub-auroral band bounded by the inflowing current and lower-latitude equatorward current. This current system, hereafter designated as the equatorial outward radial (EOR) system, is fundamentally a planetary-rotation-driven system and is regarded as an unlikely alternative to the current system described above in the present context (Appendix 1).

Ring Current Model Magnetosphere

A model of Saturn's magnetospheric magnetic field, constructed by superposition of the Z_3 model internal field [Connerney et al., 1982] and the field due to the ring current is compared in Figure 8 with a dipolar magnetic field. Figure 8 is a meridional profile of magnetospheric field lines, illustrating the moderate distension of field lines in the equatorial plane. Field lines are labeled with the co-latitude appropriate to the foot of the field line in the northern hemisphere The resulting geometry has been used successfully to relate charged particle absorption signatures to satellites and rings [Acuña et al., this issue] and better organize Voyager high energy charged particle fluxes [Schardt and McDonald, this issue] throughout Saturn's magnetosphere.

The model magnetosphere is axisymmetric, reflecting the axial symmetry of both the Z_3 internal field model and the field due to the ring current. Asymmetries due to the magnetopause boundary and tail current systems driven by the solar wind interaction, not included in the model, become evident in the Voyager magnetic field obsevations at radial distances greater than $\sim$ 15 R_S (outbound). Comple ` absence of data at low latitudes deep within Saturn's magnetic tail frustrates attempts to describe quantitatively the field geometry there. Thus far, magnetotail currents have been inferred from high latitude observations. Behannon et al. [1981] constructed a semi-quantitative model of Saturn's magnetosphere consistent with the Voyager 1 magnetic field observations and closure of field lines across the tail as indicated by the observed electron pitch angle distributions [Krimigis et al., 1981].

Saturn's magnetospheric configuration appears more similar to the earth's than the disc-like Jovian magnetosphere. The total integrated ring current in Saturn's magnetosphere is $\approx 10^7$ A, only a few percent of the total current of the Jovian magnetodisc [Connerney et al., 1981a] and approximately an order of magnitude greater than the earth's quiet time ring current [Hoffman and Bracken, 1965]. Connerney et al. [1981b] demonstrated that these three very dissimilar magnetospheres each have near-axis (ring current) perturbation fields ΔB of $\sim 5 \times 10^{-4}$ B_e, where B_e is the planet's equatorial field strength. The planetary and ring-current fields of Earth, Saturn, and Jupiter are summarized in Table 2 along with an estimate of the total ring current in each magnetosphere. The earth's ring current appears to be considerably more variable than either Jupiter's or Saturn's. An estimated ΔB of 10-23 nT [Mead and Fairfield, 1975] is considered to be representative of the earth's quiet-time ring current. Langel et al. [1980] found a ΔB of 20.4 nT from an analysis of two days (November 5-6, 1979) of Magsat observations. On the basis of data obtained from just two or three spacecraft encounters with Jupiter and Saturn, it appears that the remaining estimates of ΔB in Table 2 have an uncertainty of $\approx$ 20%.

The Dessler-Parker relation [Dessler and Parker, 1959; Carovillano and Siscoe, 1973] links the quantity $\Delta B/B_e$ to the ratio of the kinetic energy of trapped particles in the magnetosphere (E) and the dipole magnetic energy

outside the planet's surface (U). While the ratio E/U for the three magnetospheres is approximately equal, the equatorial field strength and thus the total kinetic energy (E) varies by orders of magnitude. The predictive capabilities of scaling laws for planetary magnetic fields are less than satisfactory. However, once a planetary equatorial field strength is determined, Table 2 suggests that the ring-current perturbation field is relatively well determined.

Magnetospheric Plasma

Some properties of the plasma trapped in Saturn's magnetosphere can be inferred from a model of the magnetospheric magnetic field through the use of a magnetohydrodynamic formulation. Such a model has been utilized by several authors [Gleeson and Axford, 1976; Liu, 1982; Goldstein, 1977; Goertz, 1979; Vasyliunas, 1983; for a review see Vasyliunas, 1983] to deduce plasma properties of the Jovian magnetodisc. This approach provides useful information about gross plasma properties but does not in itself address issues which require a consideration of individual particle motion, e.g., charged particle absorption phenomena. Individual particle motion in the distended magnetospheres of Jupiter and Saturn is discussed by Birmingham [1982].

In the magnetohydrodynamic (MHD) formulation the magnetospheric plasma is treated as a conducting, compressible fluid entrapped in the rapidly rotating magnetosphere. In the steady state, with isotropic pressure $p(\rho, z)$, mass density $\delta(\rho, z)$, and velocity $\vec{V}(\rho, z)$, the plasma force balance is expressed by

$$\delta(\vec{V}\cdot\vec{\nabla})\vec{V} = \vec{J} \times \vec{B} - \vec{\nabla}p \qquad (1)$$

neglecting viscous and gravitational forces. In rotating coordinates, assuming corotation, axial symmetry, and azimuthally directed currents, equation (1) reduces to two equations relating the plasma pressure and mass density to the magnetospheric magnetic field and current density:

$$-\delta\ \rho\omega^2 = -\frac{\partial P}{\partial \rho} + J_\phi\ B_z \qquad (2)$$

$$0 = -\frac{\partial P}{\partial z} - J_\phi B_\rho \qquad (3)$$

With the magnetic field and current density given by the ring current model, the pressure and mass density in Saturn's magnetosphere can be calculated subject to suitable boundary conditions. Assuming that $P \to 0$ as $z \to \pm \infty$, the ring current model taken at face value implies that $P \to 0$ at the surface bounding the model ring current in $\hat{z}$. Thus,

$$P(\rho,z) = \int_z^{(\mathrm{sgn}\ z)D} J_\phi B_\rho \, dz' \qquad (4)$$

Taking $J_\phi = I_o/\rho$ and $I_o = 2.9 \times 10^6$ A/R_S for Saturn, plasma pressures at the equator and at $z = 1,2$ for $8 < \rho < 15.5$ have been evaluated numerically and are shown in Figure 9. The plasma pressure in the equatorial plane decreases from $\sim 27 \times 10^{-10}$ dynes/cm^2 at $\rho = 9$ R_S to $\sim 4 \times 10^{-10}$ dynes/cm^2 at $\rho = 15$ R_S.

Similarly, evaluation of

$$\sigma(\rho) = \int_0^D \delta(\rho,z') \, dz'$$

using equations 2 and 4 results in an estimate of the height-integrated plasma mass density in Saturn's magnetosphere. The mass density decreases from $\sim 1.1 \times 10^{-11}$ Kg/m^2 at $\rho = 9$ R_S to $\sim 5.4 \times 10^{-12}$ Kg/m^2 at $\rho = 15$ R_S. In this region, Bridge et al. [1981] identified a heavy ion species with mass to charge ratio of 14–16 as the dominant ion species. An effective ion number density estimate, N_e, is obtained from the mass density by assuming an ion species with atomic mass of 16 a.m.u. (oxygen) and uniform distribution throughout the ring-current region. The inferred plasma mass density and ion number density are shown in Figure 10. In Figure 11 we compare our estimated ion density with the ion densities obtained by Frank et al. [1980] from Pioneer 11 observations made near the equatorial plane, and the equatorial ion

density inferred by Bridge et al. [1982] from Voyager 1 and 2 plasma observations (of electron density) at higher latitudes. At ring-current radial distances, there is, in general, a rather good agreement among all three estimates of ion density. The ion density estimated from the model magnetic field is consistently greater than those of the plasma experiments. However, Frank et al. [1980] reported difficulty in identifying the ion species in this region but assigned a mass per charge ratio of 1 (H^+) to the ions within the radial range of 10-16 R_S. If we attribute the mass density obtained from the model magnetosphere to H^+ ions, the required number densities would be 16 times that shown in Figure 11, at variance with the observed ion densities. Agreement between the two ion density estimates is achieved only if the ions have a large mass to charge ratio, in agreement with the results of the Voyager plasma investigation [Bridge et al., 1981; 1982]. An ion density estimate based on equation (1) might be greater than those of the plasma experiments if some fraction of the charged particles escape detection by the plasma experiments, e.g., if the ion species is too cold to be measured far above the equatorial plane or perhaps energetically outside the range of the available detectors. The plasma pressure and integrated mass density obtained here are both more reliable than the quoted effective ion density, which required additional assumptions. Particles not contributing significantly to the mass density have been neglected in this approximation.

Additional practical considerations limit the usefulness of equation (1) in obtaining plasma properties from a specific magnetic field model. Close to the planet, where the radial magnetic field is dominated by internal sources, even a small azimuthal current density J_ϕ may contribute significantly to the pressure by virtue of equation (4). Such a small current density may not be evident in the observed magnetic field. Thus, in regions where the magnetic field of internal origin is much greater than that due to plasma currents (for Saturn, $\rho \lesssim 8\ R_S$) the plasma pressure is difficult to estimate. In Saturn's magnetosphere, for example, only $\sim$ 30% ($\sim$ 13%) of the current density at $\rho = 8$ is required to obtain the same pressure at $\rho = 6$ ($\rho = 5$). Regions where $J_\phi = 0$ (outside the ring current region illustrated in Figure 8) should not be interpreted (literally) as implying a vanishing pressure.

The boundary conditions essential to equation (4) require $P \to 0$ at $z = \pm D$ since $\partial P/\partial z = 0$ outside the current carrying region ($J_\phi = 0$) and $P(z \to \infty) = 0$. However, if we allow a very small J_ϕ at $|z| > D$, it is clear that the condition $P(z \to \infty) \to 0$ can be satisfied for non-zero $P(z = \pm D)$. To the right hand side of equation (4) we are thus free to add a suitable function $P^*(\rho)$. While $P^*(\rho)$ is apt to be a small fraction of the $P(\rho,z)$ of equation (4), there is no assurance that $\partial P^*/\partial\rho$ is likewise small so the mass density estimate must be regarded more cautiously. Finally, we have computed a height-integrated mass density to reduce the dependence of the result on the assumed distribution of current in $\hat{z}$ since the model quantity $J_\phi \times D$ (total height-integrated current at radial distance ρ) is better determined than either term independently [Connerney et al., 1981 a,b). Note that the mass density $\delta(\rho,z)$ is the difference of the two quantities $\partial P/\partial\rho$ and $J_\phi B_z$ and that small uncertainties in either can result in large uncertainties in $\delta(\rho,z)$. The computed plasma pressure is already relatively insensitive to the detailed distribution of current in $\hat{z}$ or the model parameter uncertainties and as such is estimated with more confidence.

Summary

Saturn's magnetosphere is unique in the remarkable axisymmetry of its internal field. In the neighborhood of the Voyager closest approach distances of 2.7-3 R_s, the observed magnetic field is consistent with axisymmetry to within a nT or 2, or to the level of $\sim$ 0.2% of the total field. This is much less than the field of the ring current ($\sim$ 10 nT) and probably comparable to the near axis field due to magnetopause and tail currents. The daily variation of the orientation of the terrestrial and Jovian dipoles with respect to the planet-sun line ($\pm$ 11.7° and $\pm$ 9.6°, respectively) is reproduced at Saturn on the much longer time scale of Saturn's sidereal period, approximately 30 years. Thus Saturn's magnetosphere may be an ideal laboratory for the study of magnetospheric processes and the interaction of the solar wind with a planetary magnetosphere.

Estimates of the plasma pressure and mass distribution in Saturn's magnetosphere obtained from the ring current magnetic field model are reasonably consistent with those obtained by the Voyager and Pioneer plasma

experiments. A consideration of detailed particle motion in such a magnetospheric magnetic field [e.g., Birmingham, 1982] and the in situ plasma observations should lead toward an improved current distribution (and model magnetosphere). From the MHD stress balance it is clear that the plasma pressure or mass density measured on the spacecraft trajectory contains information about the azimuthal current density and magnetic field far from the point of observation. In this respect use of plasma observations to constrain or improve magnetospheric models is similar to the use of charged particle absorption signatures to infer the geometry of a magnetic field line.

The Dessler-Parker relation establishes a rather generally applicable relationship between the quantity $\Delta B/B_e$ and E/U, where E is the total kinetic energy of trapped particles in the magnetosphere and U is the dipole magnetic energy exterior to the planet's surface. Observations at the earth, Jupiter, and Saturn are consistent with a constant ratio $\Delta B/B_e$ (5×10^{-4}) among planetary magnetospheres. This empirical result implies that each planetary magnetosphere acquires a trapped particle population with a total kinetic energy of 5×10^{-4} U, that is, a fixed percentage of the available magnetic field energy external to the planet.

Acknowledgments

We thank our Voyager colleagues and our colleagues at the NASA/Goddard Space Flight Center for useful discussions, particularly D. P. Stern at GSFC. We also thank F. Hunsaker, L. White and the data processing and technical support staff at Goddard for their assistance, and two referees for useful comments.

APPENDIX 1
DISCUSSION OF THE EOR CURRENT SYSTEM

Within the context of the (axially symmetric) EOR system, the observed radial dependence of the azimuthal field for $\rho < 10\ R_s$ requires current injection in the equatorial plane to occur at low L values (McIlwain's 'L' parameter), below the minimum $L \sim 4.3$ reached by Voyager 1. Current closure occurs between there and $\sim 72^\circ$ latitude or entirely at higher latitudes, depending on model assumptions. This requires a $\lesssim 10^\circ$ latitude path in Saturn's relatively poorly conducting sub-auroral ionosphere. We estimate the height-integrated Pedersen conductivity Σ_s of Saturn's sub-auroral ionosphere to be of order .1 mho, with an upper limit of ~ 1 mho (Appendix 2). The total current I at a co-latitude θ flowing in response to an electric field E is given by $I = 2\pi R_s \sin\theta\ \Sigma_s E$ where R_s is the radius of Saturn. We have neglected the (relatively small) latitudional dependence of the horizontal conductivity at high latitudes in using $\Sigma = \Sigma_s$. Assuming that the system is driven by planetary rotation, the available $E(\theta)$ is a fraction α (describing the lack of corotation) of the $\vec{V}x\vec{B}$ where $V = r\Omega$ and B is the magnetic field at the point along the field line where E is evaluated. Applied at the ionosphere, assuming a dipole field, $I(\theta) = 4\pi R_s^2\ \alpha\Omega\Sigma_s B_o \sin^2\theta \cos\theta$, where B_o is Saturn's equatorial dipole field strength (21,000 nT). With the upper limit estimate of 1 mho for Σ_s, and $\alpha \sim 0.1$, we obtain $I(\theta) = 15\ 10^6 \sin^2\theta \cos\theta$ A. If we assume that all of the observed B_ϕ is due to the EOR system, then all of the current must have closed at latitudes $\lesssim 72^\circ$ corresponding to $\rho \gtrsim 7.2\ R_s$ where B_ϕ is reduced effectively to zero. In this case, since the ionospheric current implied by the observed B_ϕ decreases with decreasing θ more rapidly than $\sin^2\theta$, the most severe requirements for driving the current are found at the largest θ. At minimum ρ, Voyager 1 is located at $L = 5.4$ (or 25°) where our upper limit estimate $I(25^\circ) = 2.7 \times 10^6$ A, somewhat less than the current of 7×10^6 A required by the maximum B_ϕ observed.

If instead we assume that the constant term in the least squares fit to B_ϕ is due to magnetopausse and/or magnetotail currents, a somewhat lower estimate results. The sign and magnitude of the (-4.6 nT) constant B_ϕ term is consistent with a magnetopause/magnetotail field when the latitude and local time of Voyager 1's trajectory are taken into account. In this case, all of the EOR return currents must close at high ($\gtrsim 70^\circ$) latitudes, where the estimated upper limit $I(\theta = 20^\circ)$ is $\sim 1.7 \times 10^6$ A. This is considerably less than the 9×10^6 A required by the coefficient 33.3 nT-R_s of the least squares fit.

APPENDIX 2

ESTIMATE OF IONOSPHERIC CONDUCTIVITY AT SATURN

The current density $\bar{J}$ in a weakly ionized gas is

$$\bar{J} = \sigma_o \bar{E}_w + \sigma_p \bar{E}_\perp + \sigma_H (\bar{B}x\bar{E})/B$$

where $\bar{E}_w$ and $\bar{E}_\perp$ are the components of the electric field vector $\bar{E}$ parallel to and perpendicular to the magnetic field $\bar{B}$. The Pedersen σ_p and Hall σ_H conductivities are given by [e.g., Akasofu and Chapman, 1972]

$$\sigma_p = e^2 n_e \left[\frac{\nu_{in}}{m_i (\omega_i^2 + \nu_{in}^2)} + \frac{\nu_{en}}{m_e (\omega_e^2 + \nu_{en}^2)}\right] \qquad A1$$

and

$$\sigma_H = e^2 n_e \left[\frac{\omega_e}{m_e (\omega_e^2 + \nu_{en}^2)} - \frac{\omega_i}{m_i (\omega_i^2 + \nu_{in}^2)}\right] \qquad A2$$

where e is the electron charge, n_e the number density of charaged particles, $m_e(m_i)$ the mass of an electron (ion) with gyrofrequency ω_e (electron) and ω_i (ion); ν_{in} and ν_{en} are the collision frequencies of ions with neutrals and electrons with neutrals. Gyrofrequencies of electrons and ions are $\omega_e = eB/m_e$ and $\omega_i = eB/m_i$ respectively in a magnetic field B.

The number density of charged particles n_e at ionospheric altitudes in Saturn's atmosphere has been deduced from the Pioneer 11 [Kliore et al., 1980] and Voyager radio occulations [Tyler et al., 1981; 1982]. The number density n_e as a function of altitude (referenced to the 1 bar level in Saturn's atmosphere) obtained from the high-latitude Voyager 1 occultation is illustrated in Figure A1 along with the computed H^+ ion and electron

gyrofrequencies. The number density deduced from the low latitude Pioneer 11 occultation showed less variation with altitude reaching a maximum of $\sim 10^4$ cm^{-3} at $\sim$ 1.5 to 2 10^3 km altitude. The electron density is considered to be controlled by incident solar ultraviolet radiation and generally an order of magnitude less than expected on the basis of current models of Saturn's ionosphere [Atreya and Waite, 1981]. The electron-neutral and ion-neutral collision frequencies appearing in equations A1 scale linearly with neutral particle density n [Dalgarno, 1961]. The neutral particle density increases exponentially with decreasing altitude, so the relevant collision frequency also increases exponentially with decreasing altitude, as illustrated in Figure A1. The collision frequency in cycles sec^{-1} shown is that of H^+ ions in molecular hydrogen gas computed from

$$\nu_{in} = 1.86 \times 10^{-9} \, n \qquad \text{(A3)}$$

the neutral number density n in cm^{-3} is from the model of Atreya and Waite [1981]. Equation A3 results from equations given by Dalgarno (1961) with the polarizability of molecular hydrogen (α_o = 5.44 in atomic units) from Venanzi and Kirtman [1973]. For the purpose of estimating the Pedersen conductivity it is sufficient to note that σ_p is essentially determined by the electron density in the region where ν_{in} and ω_i are comparable, i.e., just below 1000 km relative altitude. Similarly, the largest contribution to the height integrated Pedersen conductivity $\Sigma = \int \sigma \cdot dh$ will be confined to an altitude band of $\lesssim$ 500 km depth over which the number density of neutrals varies by more than an order of magnitude. Unfortunately, $\nu_{in} \sim \omega_i$ well below the $\sim$ 1800 km altitude probed by spacecraft observations. One must therefore attempt to estimate n_e at lower altitudes, in spite of the very limited success of current theoretical models of Saturn's ionosphere [Atreya and Waite, 1981]. Such an estimate is very tentative without electron density measurements at lower altitudes. Thus an upper limit for Σ_s, assuming that n_e has decreased to $\sim 10^3$ cm^{-3} at 1000 km and a magnetic field magnitude of 60,000 nT, is $\sim$ 1 mho. A more realistic estimate of Σ_s for Saturn's ionosphere is perhaps of order 0.1 mho. Siscoe [1979] estimated Saturn's Σ to be Σ_s = 0.2 mho, prior to the availability of electron density or magnetic field observations, by reducing an estimate of Jupiter's Σ_J by the ratio of heliocentric distances.

TABLE 1

ORIGINAL PAGE IS
OF POOR QUALITY

	Variable External Field (nT)		Z_3 (nT)
		(V1) (V2)	
ε_1^0	21509		21535
ε_2^0	1603		1642
ε_3^0	2827		2743
G_1^0	-11	-9	- 10
G_1^1	-1	-1	-1
H_1^1	3	-2	0

TABLE 2

MAGNETOSPHERE	B_o (G)	ΔB(nT)	$\Delta B/B_o$	I(A x 10^6)
Earth	.31	10–23	$(3.3\text{–}7.5)\times10^{-4}$	0.75
Saturn	.22	10	5×10^{-4}	10
Jupiter	4.20	200	5×10^{-4}	300

References

Acuña, M. H. and N. F. Ness, The magnetic field of Saturn: Pioneer 11 observations, Science, 207, 444, 1980.

Acuña, M. H., J. E. P. Connerney, and N. F. Ness, Topology of Saturn's main magnetic field, Nature, 292, 721, 1981.

Acuña, M. H., N. F. Ness and J. E. P. Connerney, The magnetic field of Saturn: Further studies of the Pioneer 11 observations, J. Geophys. Res., 85, 5675, 1980.

Acuña, M. H., J. E. P. Connerney, and N. F. Ness, The Z_3 zonal harmonic model of Saturn's magnetosphere: Implications and Applications, J. Geophys. Res., this issue, 1983.

Akasofu, S., and S. Chapman, Solar Terrestrial Physics, Oxford Press, Oxford, p. 243, 1972.

Atreya, S.K., and J. H. Waite, Jr., Saturn ionosphere: Theoretical interpretation, Nature, 292, 682, 1981.

Atreya, S. K., J. H. Waite, Jr., T. M. Donahue, A. S. Nagy, J. C. McConnell, Theory, measurements and models of the upper atmosphere and ionosphere of Saturn, in Saturn, ed. T. Gehrels, University of Arizona Press, in press.

Baum, W. A., T. Kreidl, J. A. Westphal, G. E. Danielson, P. K. Seidelmann, P. Pascu, and D. G. Currie, Saturn's E Ring 1.) CCD observations of March 1980, Icarus, 47, 84, 1981.

Behannon, K. W., J. E. P. Connerney, and N. F. Ness, Saturn's magnetic tail: Structure and dynamics, Nature, 292, 753, 1981.

Birmingham, T. J., Charged particle motions in the distended magnetospheres of Jupiter and Saturn, J. Geophys. Res., 87, 7421, 1982.

Bridge, H. S., F. Bagenal, J. W. Belcher, A. J. Lazarus, R. L. McNutt, J. D. Sullivan, P. R. Gazis, R. E. Hartle, K. W. Ogilvie, J. D. Scudder, E. C. Sittler, A. Eviatar, G. L. Siscoe, C. K. Goertz, and V. M. Vasyliunas, Plasma observations near Saturn: Initial results from Voyager 2, Science, 215, 563, 1982.

Bridge, H. S., J. W. Belcher, A.J. Lazarus, S. Olbert, J. D. Sullivan, F. Bagenal, P. R. Gazis, R. E. Hartle, K. W. Ogilvie, J. D. Scudder, E. C. Sittler, A. Eviatar, G. L. Siscoe, C. K. Goertz and V. M. Vasyliunas, Plasma observations near Saturn: Initial results from Voyager 1, Science, 212, 217, 1981.

Carovillano, R. L., and G. L. Siscoe, Energy and momentum theorems in magnetospheric processes, Rev. Geophys. Space Phys., 11, 289, 1973.

Connerney, J. E. P., Comment on "Azimuthal magnetic field at Jupiter" by J. L. Parish, C. K. Goertz, and M. F. Thomsen, J. Geophys. Res., 86, 7796, 1981.

Connerney, J. E. P., M. H. Acuña, and N. F. Ness, Modeling the Jovian current sheet and inner magnetosphere, J. Geophys. Res., 86, 8370, 1981a.

Connerney, J. E. P., M. H. Acuña, and N. F. Ness, Saturn's ring current and inner magnetosphere", Nature, 292, 724, 1981b.

Connerney, J. E. P., N. F. Ness, and M. H. Acuña, Zonal harmonic model of Saturn's magnetic field from Voyager 1 and 2 observations, Nature, 298, 44, 1982.

Dalgarno, A., Charged particles in the upper atmosphere, Ann. Geophys., 17, 16, 1961.

Desch, M. D., Evidence for solar wind control of Saturn radio emission, J. Geophys. Res., 87, 4549, 1982.

Dessler, A. J. and E. N. Parker, Hydromagnetic theory of geomagnetic storms, J. Geophys. Res., 64, 2239, 1959.

Dungey, J. W., Interplanetary magnetic field and the auroral zones, Phys. Rev. Lett., 6, 47, 1961.

Frank, L. A., B. G. Burek, K. L. Ackerson, J. H. Wolfe and J. D. Mihalov, Plasmas in Saturn's magnetosphere, J. Geophys. Res., 85, 5695, 1980.

Gleeson, L. J. and W. I. Axford, An analytical model illustrating the effects of rotation on a magnetosphere containing low energy plasma, J. Geophys. Res., 81, 3403, 1976.

Goertz, C. K., The Jovian magnetodisc, Space Sci. Revs., 23, 319, 1979.

Goldstein, H., Theory of the plasma sheet in the Jovian magnetosphere, Planet. Space Sci., 25, 673, 1977.

Heelis, R. A., "The Polar Ionosphere", Revs. Geophys. Space Phys., 20, 567, 1982.

Hill, T. W. Inertial limit on corotation, J. Geophys. Res., 84, 6554, 1979.

Hill, T. W. Corotation lag in Jupiter's magnetosphere: A comparison of observation and theory, Science, 207, 301, 1980.

Hoffman, R. A. and P. A. Bracken, Magnetic effects of the quiet time proton belt, J. Geophys. Res., 70, 3541, 1965.

Iijima, T. and T. A. Potemra, The amplitude distribution of field aligned currents at northern high latitudes observed by Triad, J. Geophys. Res., 81, 2165, 1976.

Kaiser, M. L., M. D. Desch, J. W. Warwick, and J. B. Pearce, Voyager detection of non-thermal radio emission from Saturn, Science, 209, 1238, 1980.

Kaiser, M. L., and M. D. Desch, Saturnian kilometric radiation: Source locations, J. Geophys. Res., 87, in press.

Kliore, A. J., I. R. Patel, G. F. Lindal, D. N. Sweetnam, H. B. Hotz, J. H. Waite, Jr., and T. R. McDonough, Structure of the ionosphere and atmosphere of Saturn from Pioneer 11 Saturn radio occultation, J. Geophys. Res., 85, 5857, 1980.

Krimigis, S. M., T. P. Armstrong, W. I. Axford, C. O. Bostrom, G. Gloeckler, E. P. Keath, L. J. Lanzerotti, J. F. Carbary, D. C. Hamilton and E. C. Roelof, Low-energy charged particles in Saturn's magnetosphere: Results from Voyager 1, Science, 212, 225, 1981.

Krimigis, S. M., T. P. Armstrong, W. I. Axford, C. O. Bostrom, G. Gloeckler, E. P. Keath, L. J. Lanzerotti, J. F. Carbary, D. C. Hamilton and E. C. Roelof, Low-energy hot plasma and particles in Saturn's magnetosphere, Science, 215, 571, 1982.

Liu, Z. X., Modified disc model of Jupiter's magnetosphere, J. Geophys. Res., 87, 1691, 1982.

Langel, R. A., R. H. Estes, G. D. Mead, E. B. Fabiano, and E. R. Lancaster, Initial geomagnetic field model from Magsat vector data, Geophys. Res. Lett., 7, 793, 1980.

McDonald, F. B., A. W. Schardt and J. H. Trainor, If you've seen one magnetosphere, you haven't seen them all: Energetic particle observations in the Saturn magnetosphere, J. Geophys. Res., 85, 5813, 1980.

Mead, G. D. and D.H. Fairfield, A quantitative magnetospheric model derived from spacecraft magnetometer data, J. Geophys. Res., 80, 523, 1975.

Ness, N. F., M. H. Acuña, R. P. Lepping, J. E. P. Connerney, K. W. Behannon, L. F. Burlaga and F. M. Neubauer, Magnetic field studies by Voyager 1: Preliminary results at Saturn, Science, 212, 211, 1981.

Ness, N. F., M. H. Acuña, K. W. Behannon, L. F. Burlaga, J. E. P. Connerney, R. P. Lepping, and F. M. Neubauer, Magnetic field studies by Voyager 2: Preliminary results at Saturn, Science, 215, 558, 1982.

Parish, J. L., C. K. Goertz, and M. F. Thomsen, Azimuthal magnetic field at Jupiter, J. Geophys. Res., 85, 4152, 1980.

Scarf, F. L., D. A. Gurnett, W. S. Kurth, and R. L. Poynter, Voyager 2 plasma wave observations at Saturn, Science, 215, 587, 1982.

Schardt, A. W., and F. B. McDonald, Energetic protons and their source in Saturn's magnetosphere, J. Geophys. Res., this issue, 1983.

Simpson, J. A., T. S. Bastian, D. L. Chenette, R. B. McKibben and K. R. Pyle, The trapped radiations of Saturn and their absorption by satellites and rings, J. Geophys. Res., 85, 5731, 1980a.

Siscoe, G. L. Towards a comparative theory of magnetospheres, in Solar System Plasma Physics, Vol. 2, ed. C. F. Kennel, L. J. Lanzerotti and E. N. Parker, North Holland, 1979.

Smith, E. J., L. Davis, Jr., D. E. Jones, P. J. Coleman, Jr., D. S. Colburn, P. Dyal and C. P. Sonett, Saturn's magnetosphere and its interaction with the solar wind, J. Geophys. Res., 85, 5655, 1980.

Stern, D. P., Large scale electric fields in the earth's magnetosphere, Rev. Geophys. Space Phys., 15, 156, 1977.

Stern, D. P., The origins of Birkeland currents, Rev. Geophys. Space Phys., in press.

Thomsen, M. F. and C. K. Goertz, Reply (to comments of J. E. P. Connerney), J. Geophys. Res., 86, 7798, 1981.

Tyler, G. L., V. R. Eshelman, J. D. Anderson, G. S. Levy, G. F. Lindal, G. E. Wood, and T. A. Croft, Radio science investigations of the Saturn system with Voyager 1: Preliminary results, Science, 212, 201, 1981.

Tyler, G. L., V. R. Eshleman, J. D. Anderson, G. S. Levy, G. E. Wood, and T. A. Croft, Radio science with Voyager 2 at Saturn: Atmosphere and ionosphere and the masses of Mimas, Tethys, and Iapetus, Science, 215, 553, 1982.

Vasyliunas, V. M., 'Plasma distribution and flow' in Physics of the Jovian Magnetosphere, edited by A. J. Dessler, Cambridge Univ. Press, 1983.

Venanzi, T. J. and B. Kirtman, Calculation of the dynamic polarizability of molecular hydrogen by the distinguishable electron method, J. Chem. Phys., 58, 3953, 1973.

Vogt, R. E., D. L. Chenett, A. C. Cummings, R. L. Garrard, E. C. Strong, A. W. Schardt, J. H. Trainor, N. Lal and F. B. McDonald, Energetic charged particles in Saturn's magnetosphere: Voyager 1 results, Science, 212, 231, 1981.

Vogt, R. E., D. L. Chenette, A. C. Cummings, T. L. Garrard, E. C. Stone, A. W. Schardt, J. H. Trainor, N. Lal and F. B. McDonald, Energetic charged particles in Saturn's magnetosphere: Voyager 2 results, Science, 215, 577, 1982.

Warwick, J. W., D. R. Evans, J. H. Romig, J. K. Alexander, M. D. Desch, M. L. Kaiser, M. Aubier, Y. Leblanc, A. Lecacheux, B. M. Pedersen, Planetary radio astronomy observations from Voyager 2 near Saturn, Science, 215, 582, 1982.

Figure Captions

Fig. 1. Trajectories of Pioneer 11, Voyager 1 and Voyager 2 at Saturn in a cylindrical planetocentric equatorial coordinate system. Positions of the major satellites and rings are indicated. Stippled region is the region of model distributed (ring) currents in Saturn's magnetosphere.

Fig. 2. Comparison of modeled perturbation magnetic field with that observed by Voyager 2. Spherical coordinates (SLS) are used. Dashed curve is the magnetic field of the model ring current. Data obtained during spacecraft rolls (stippled) is omitted.

Fig. 3. Comparison of modeled perturbation field with that observed by Voyager 1. Dashed curve is the magnetic field of the model ring current.

Fig. 4. Azimuthal magnetic field component at Saturn observed by Voyager 1 at radial distances less than 10 R_s. Light line corresponds to data obtained during a spacecraft roll maneuver. Dashed line illustrates a $1/\rho$ dependence of the magnetic field.

Fig. 5. Equatorial plane projection of Voyager 1 and 2 spacecraft trajectories at Saturn. Coordinates are radial distance as a function of local time. Voyager 1 azimuthal field vectors shown at hour intervals along the trajectory. The positions of the major satellites Mimas, Enceladus, Tethys, Dione and Rhea at the time of Voyager 1 closest approach (23:45, day 317) are indicated.

Fig. 6. View of Saturn's south pole and the proposed auroral current system, consisting of an inflowing field-aligned current at 21.3 hours local time, an auroral electrojet, and current outflow in the early morning sector.

Fig. 7. Comparison of modeled perturbation magnetic field with that observed by Voyager 1, for a model containing the ring current (as in Figure 3) plus the field-aligned current system illustrated in Figure 6.

Fig. 8. Meridian plane projection of magnetosphere field lines at 2° increments of co-latitude (solid) using the Z_3 model internal field and the ring current model discussed in the text. Field lines are labeled with the co-latitude appropriate to the foot of the field line in the northern hemisphere. Field lines drawn using the Z_3 internal field and no ring current (dashed) are given at 4° increments for comparison.

Fig. 9. Plasma pressure in the equatorial plane (z=0) and above (z=1,2) at radial distances of 8 to 16 R_S in Saturn's magnetosphere computed from the ring current model magnetosphere.

Fig. 10. Height-integrated plasma mass density and equivalent number density at radial distances of 8 to 16 R_S in Saturn's magnetosphere computed from the ring current model magnetosphere.

Fig. 11. Comparison of the ion density in Saturn's magnetosphere computed from the ring current model magnetosphere with the ion densities obtained by the Pioneer 11 and Voyager plasma experiments. Radial positions of the satellites Enceladus, Tethys, Dione, and Rhea as indicated. (Adapted from Bridge et al., [1982].)

Fig. A1. Collision frequency of H^+ ions in molecular hydrogen gas and gyrofrequencies (H^+ ions and electrons) as a function of altitude referenced to the 1 bar pressure level. The electron density (solid line) deduced from the Voyager 1 radio occulation and that modeled (dashed) by Atreya and Waite [1981]. The electron density below 1800 km (short dashed) is simply extrapolated from the radio science measurements.

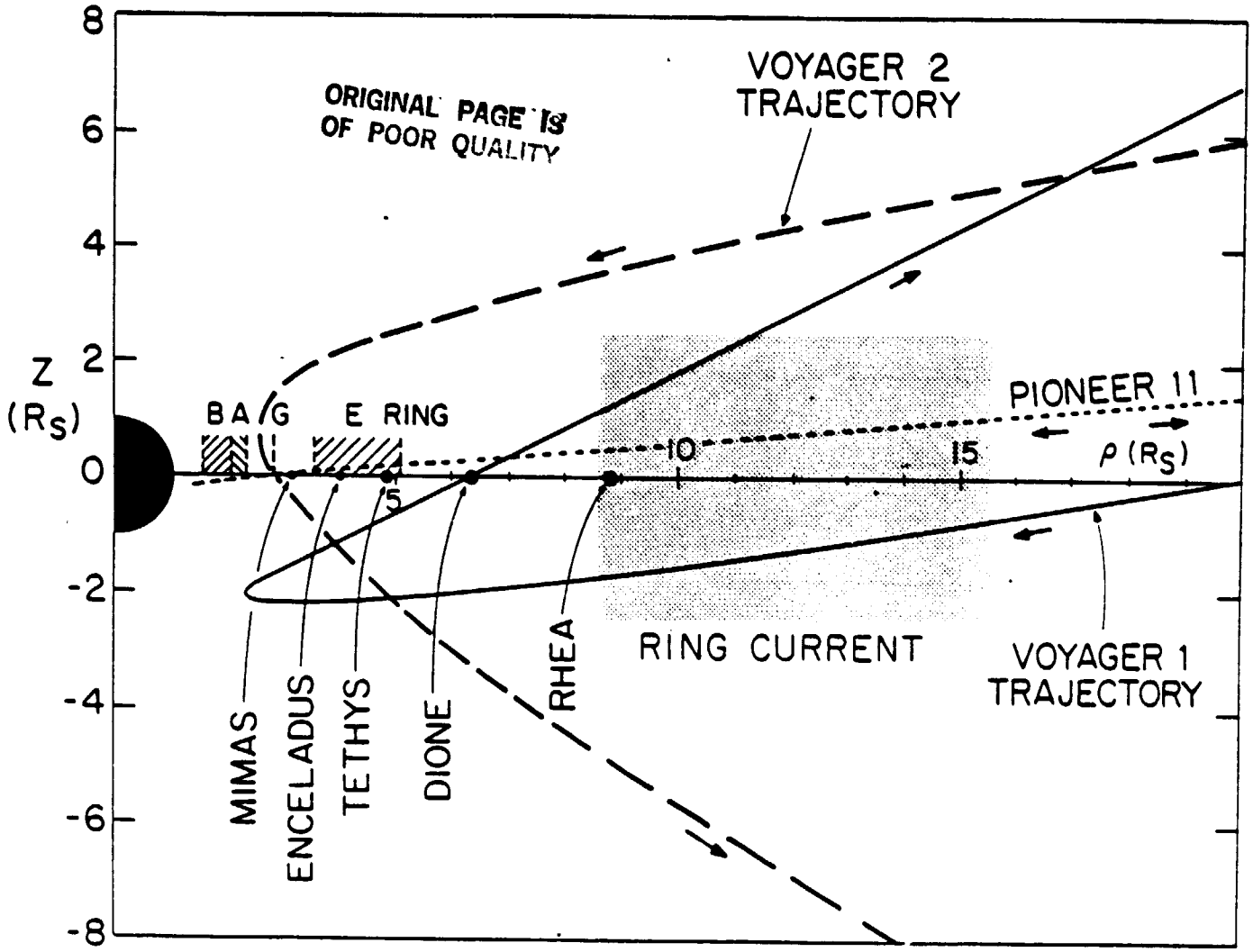
ORIGINAL PAGE IS
OF POOR QUALITY
VOYAGER 2
TRAJECTORY
PIONEER 11
Z
(Rs)
B A G
E RING
10
15
ρ (Rs)
5
RING CURRENT
VOYAGER 1
TRAJECTORY
MIMAS
ENCELADUS
TETHYS
DIONE
RHEA
8
6
4
2
0
-2
-4
-6
-8

Figure 1

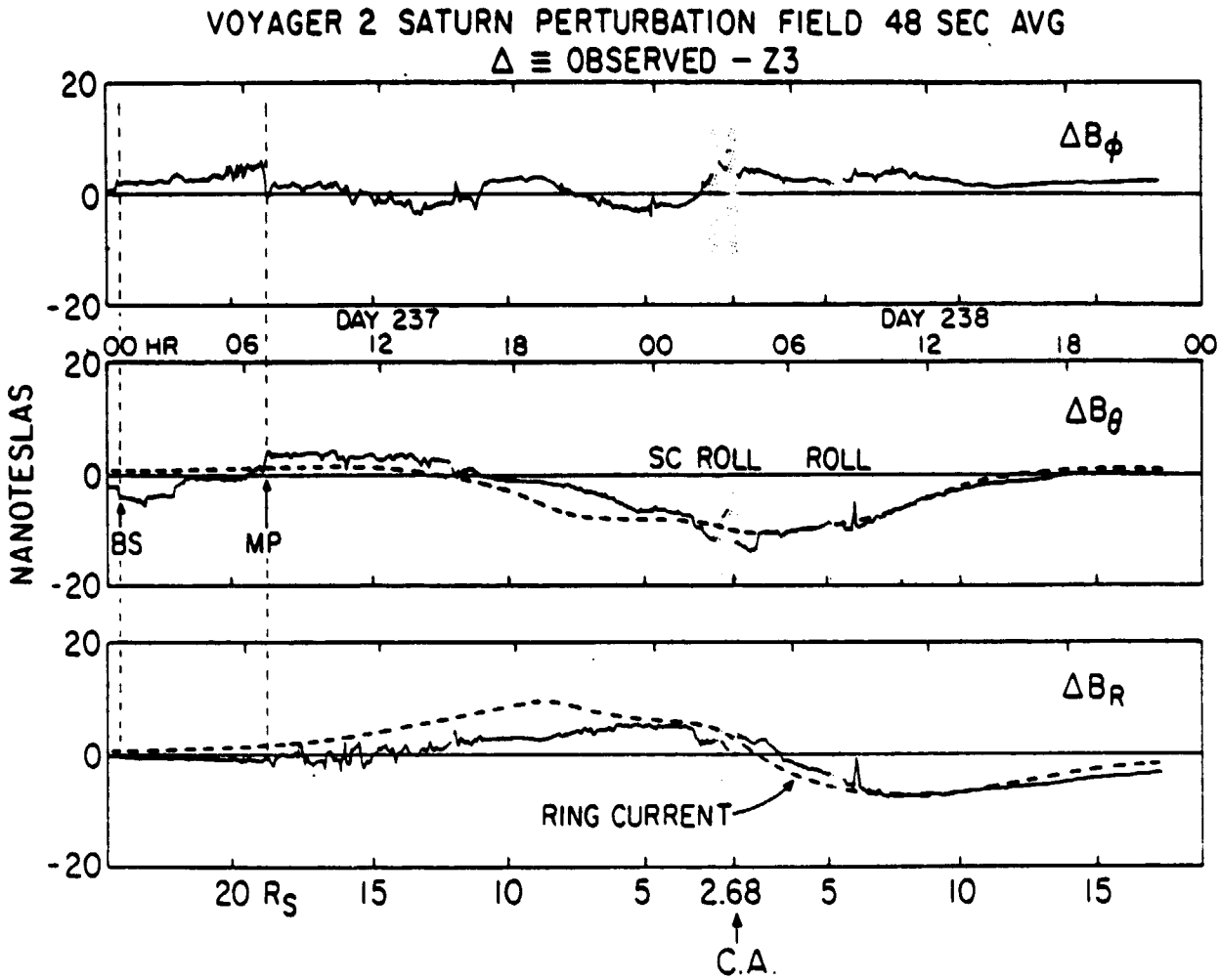

Figure 2

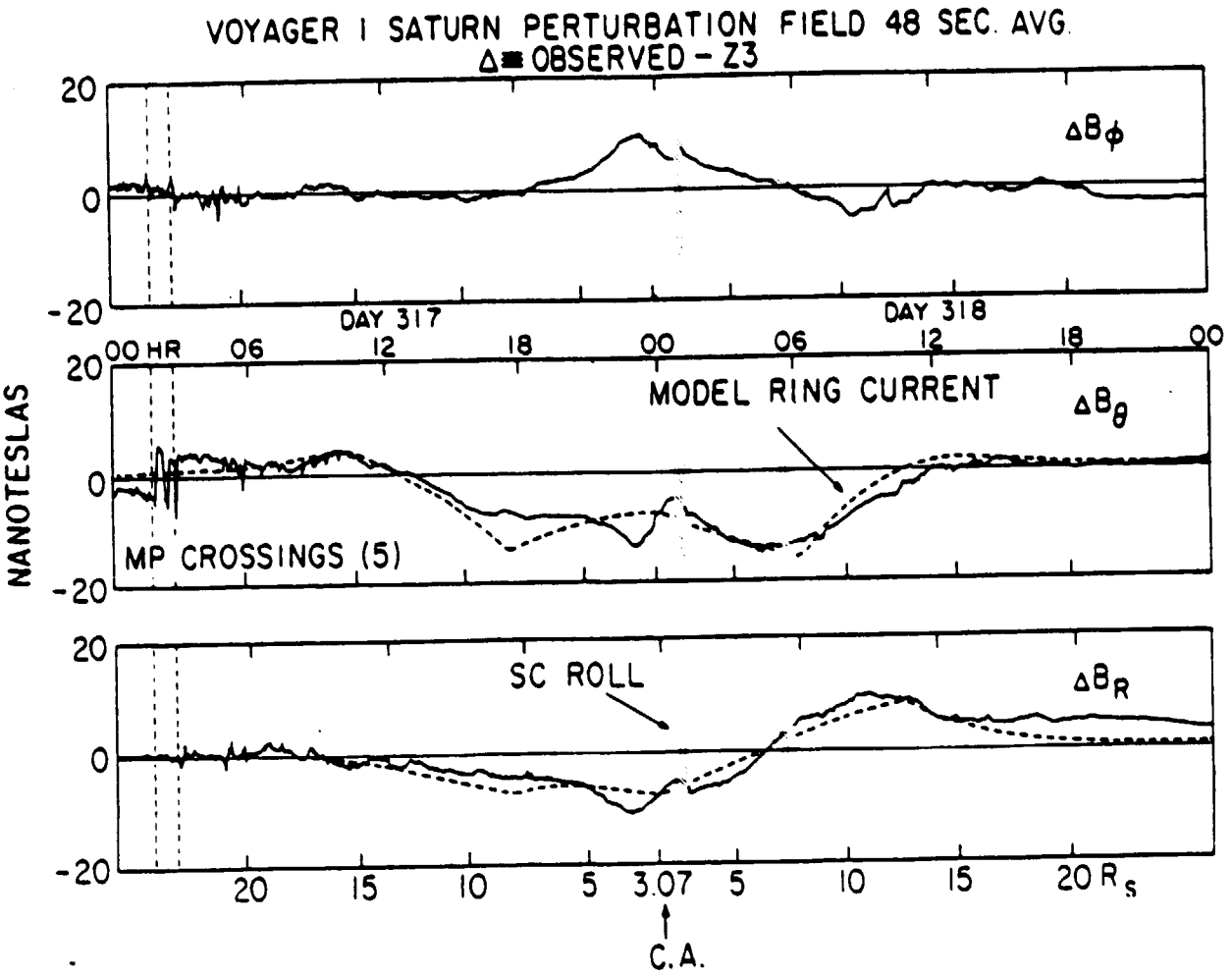

Figure 3

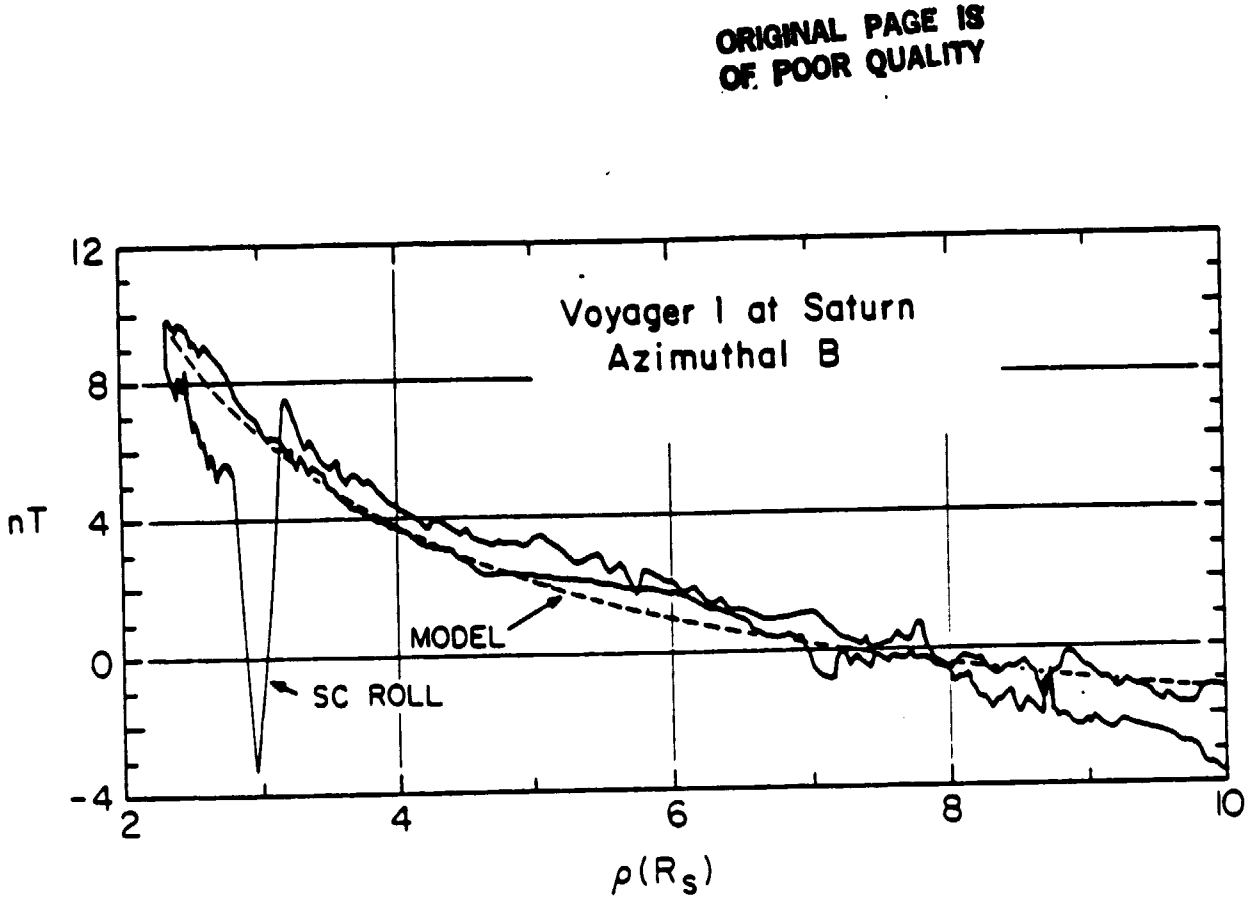

Figure 4

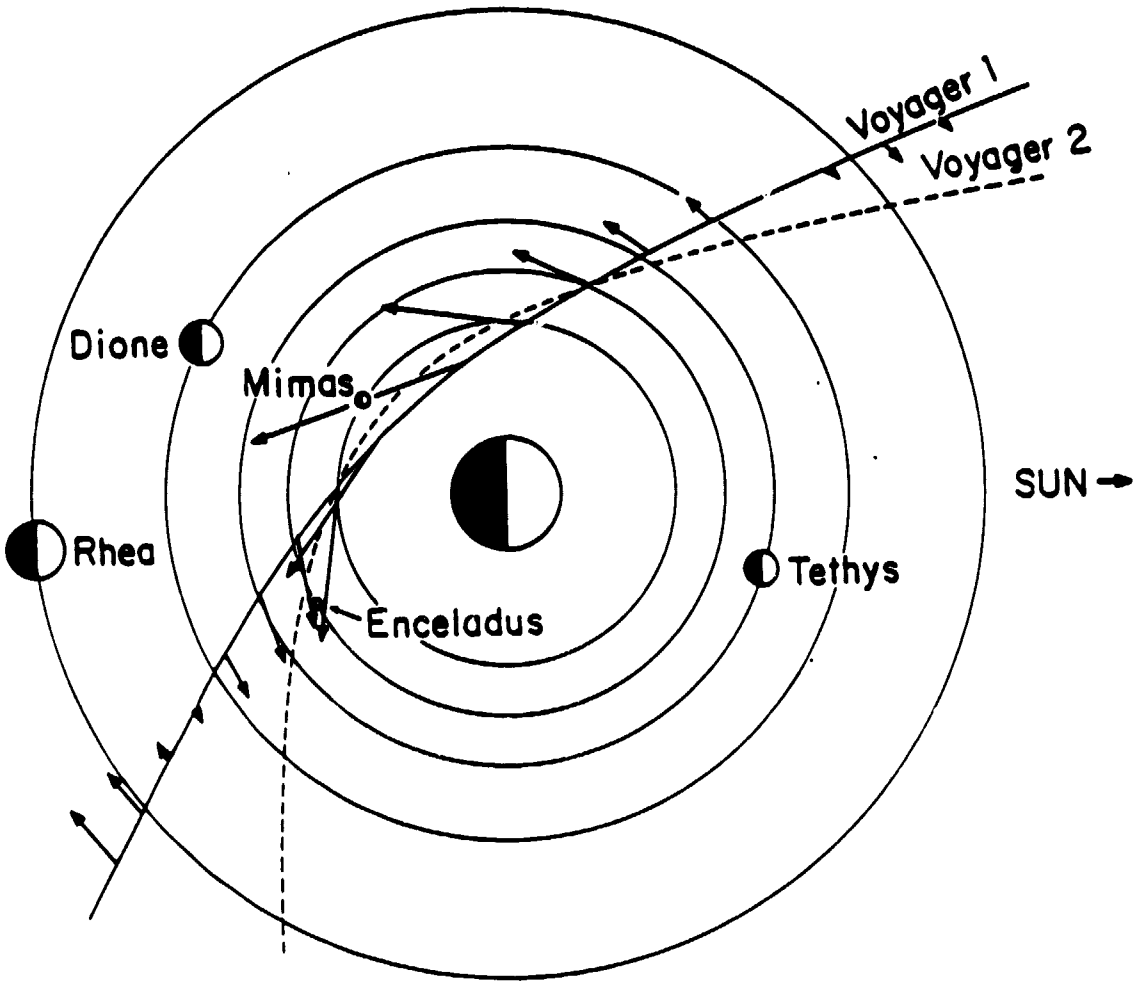

Figure 5

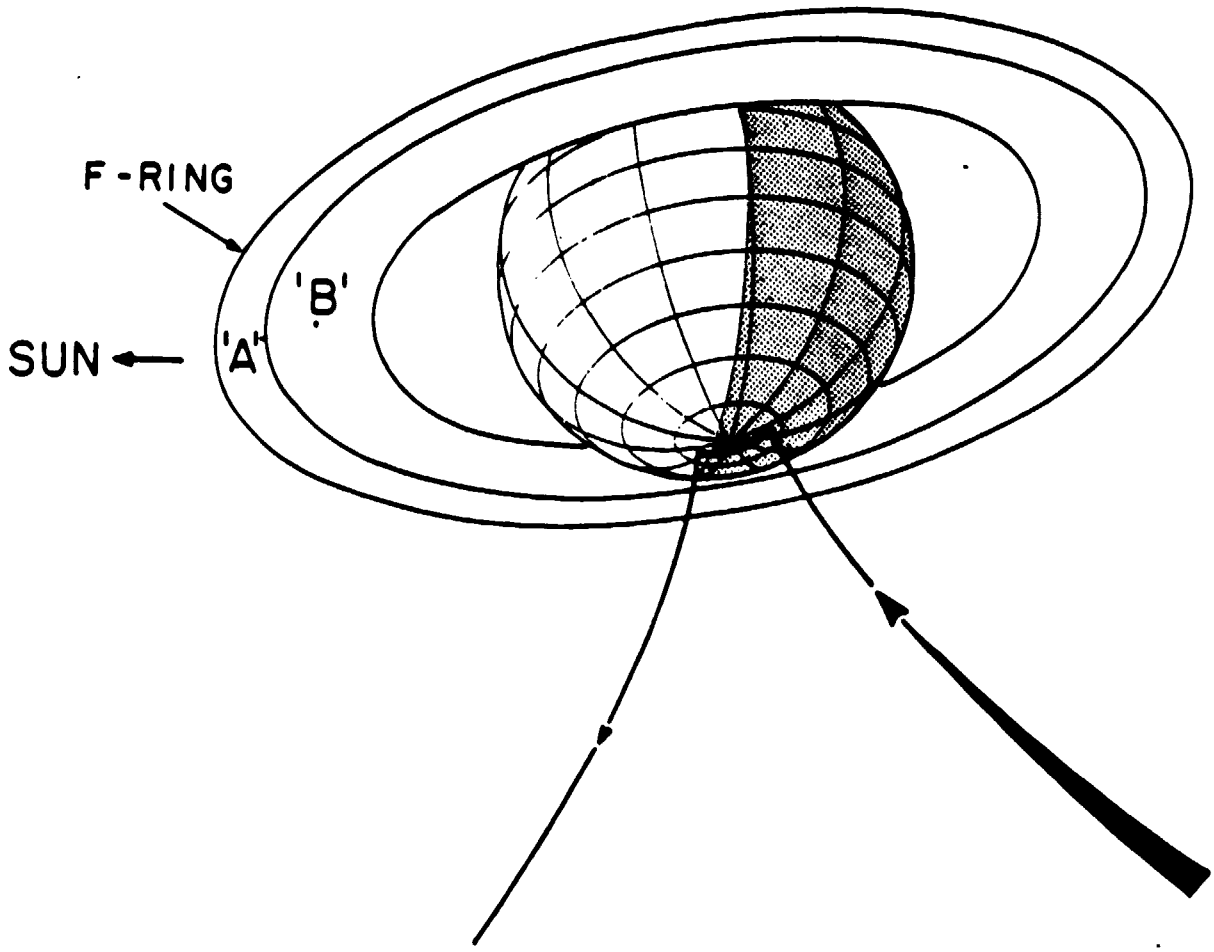

Figure 6

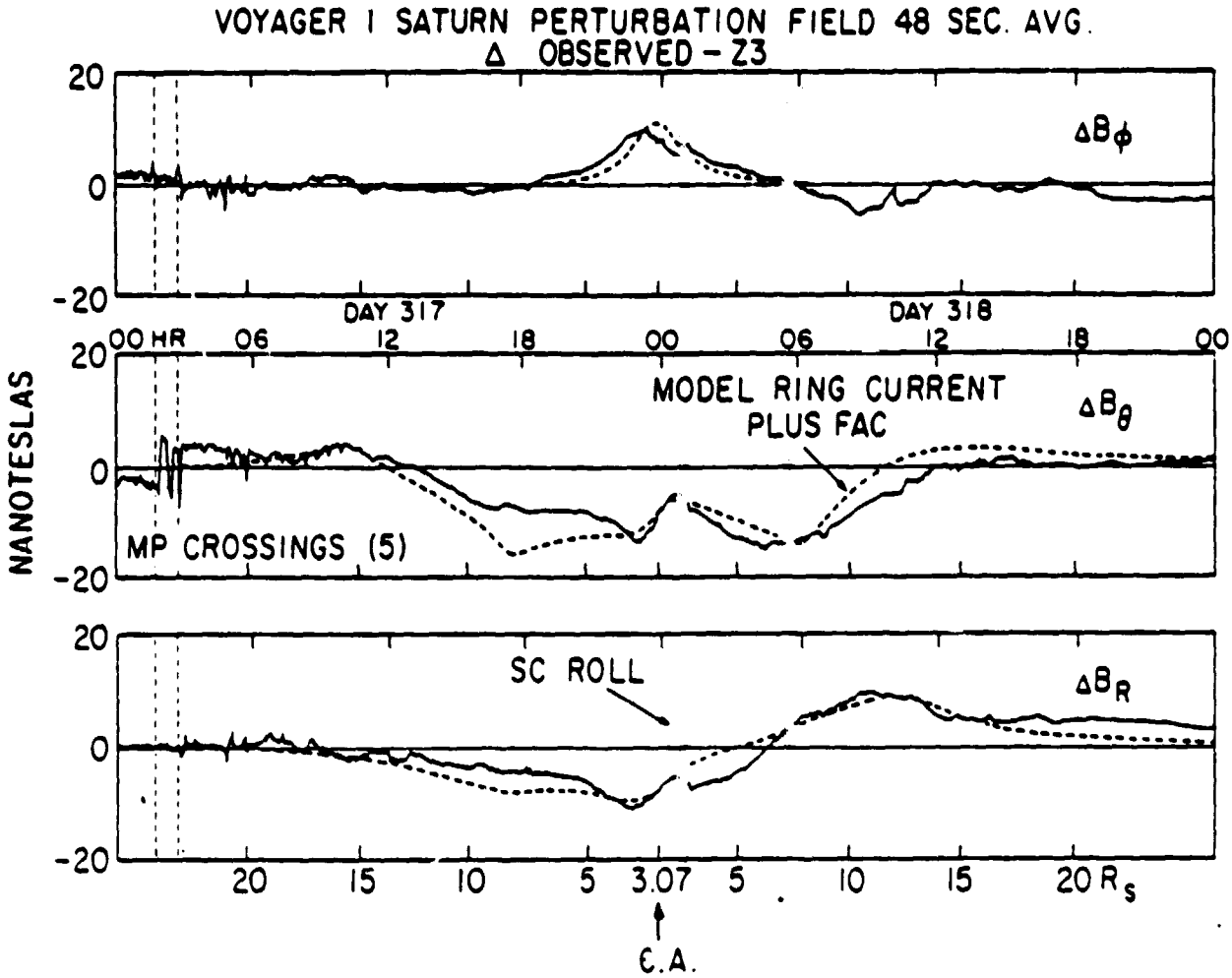

Figure 7

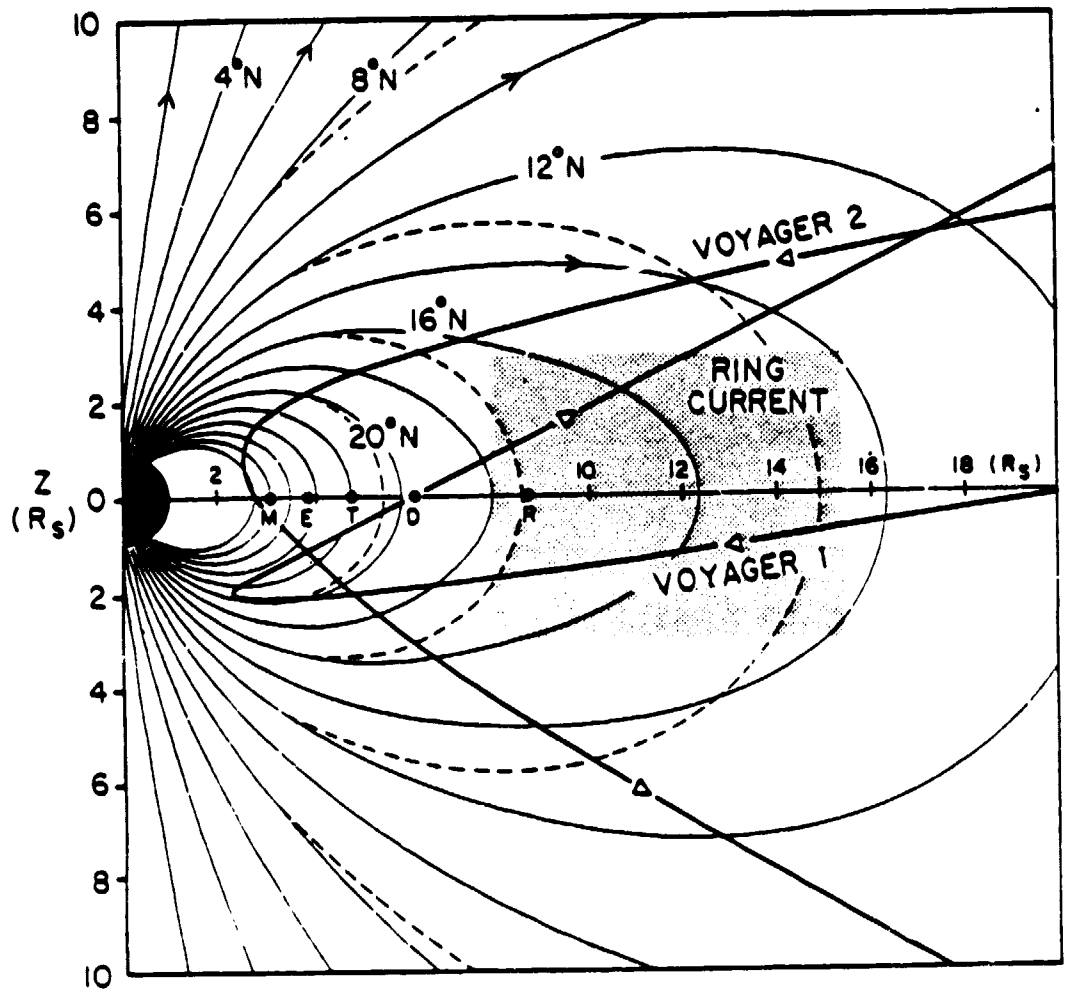

Figure 8

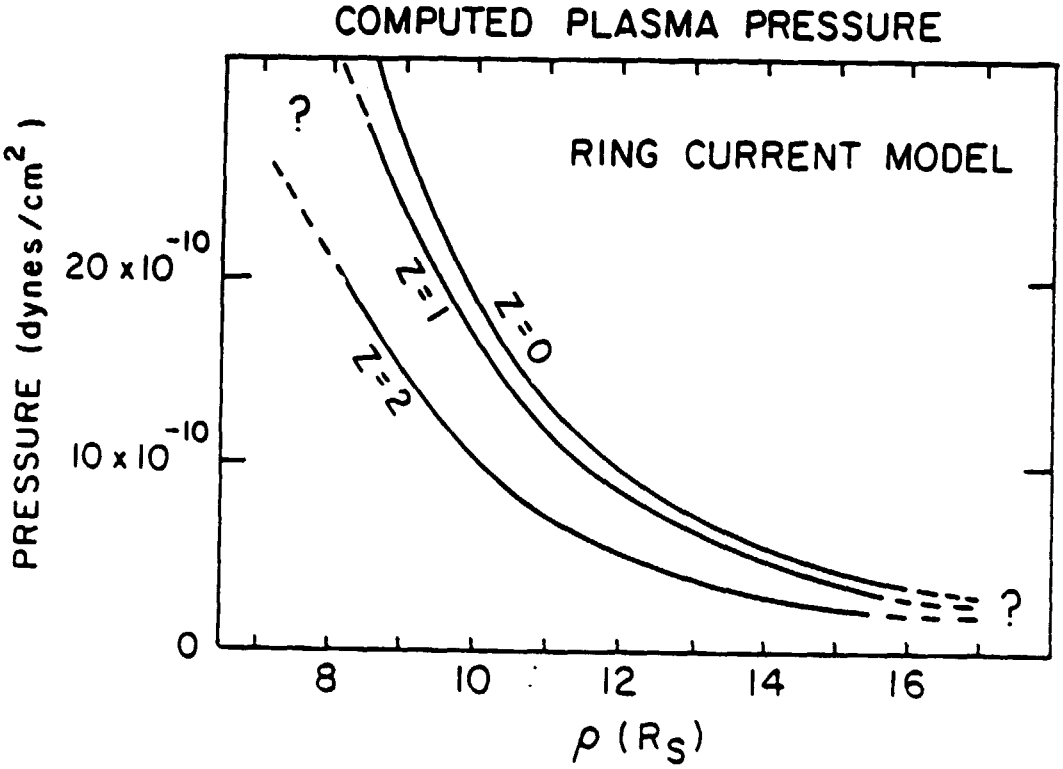

Figure 9

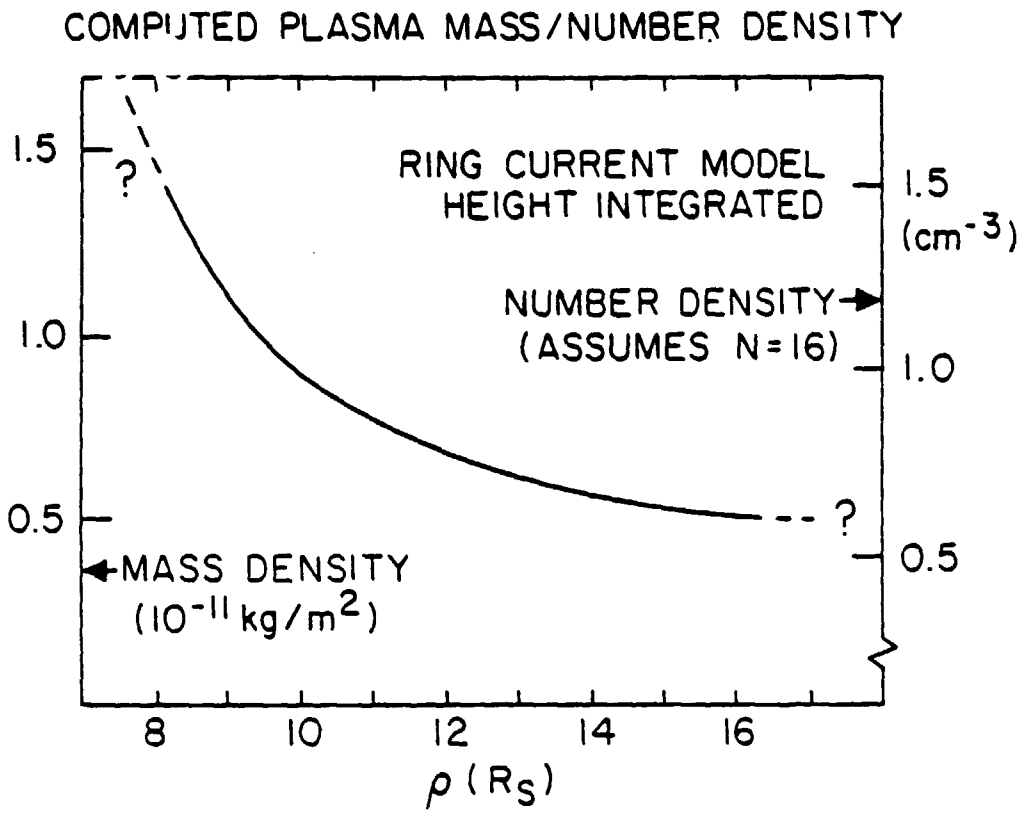

Figure 10

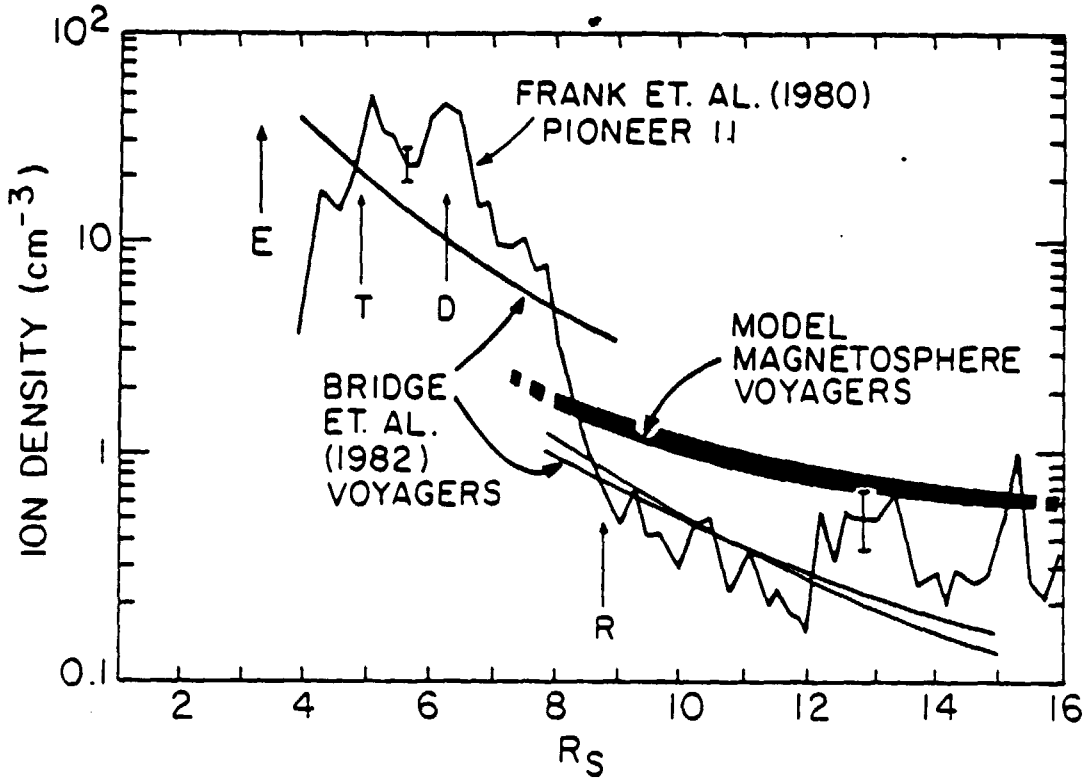

Figure 11

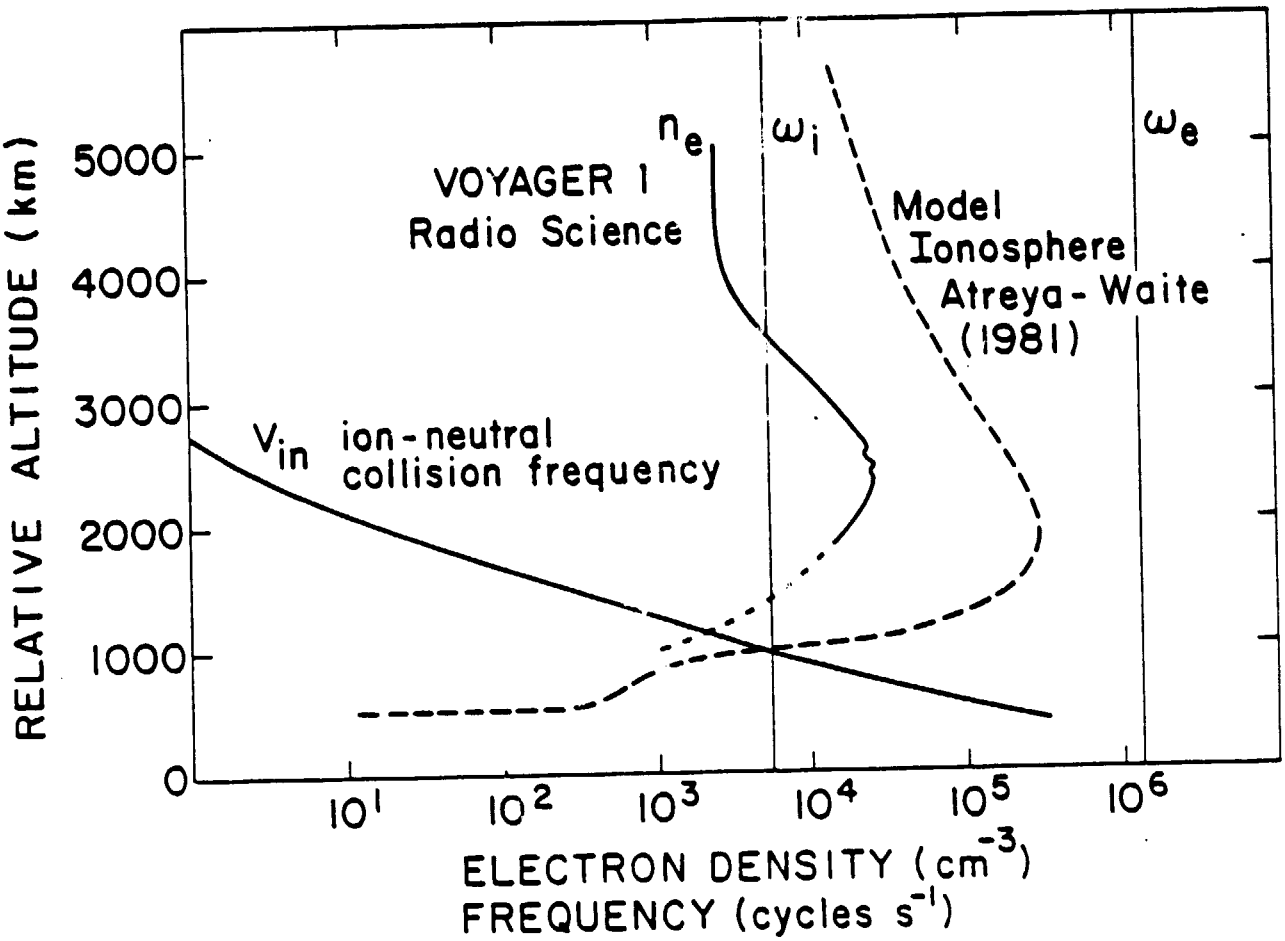

Figure A1